

On The Photodesorption of CO₂ Ice Analogues: The Formation of Atomic C in The Ice and the Effect of The VUV Emission Spectrume

N.-E. SIE,¹ G.M. MUÑOZ CARO,² Z.-H. HUANG,¹ R. MARTN-DOMNECH,³ A. FUENTE,⁴ AND Y.-J. CHEN¹

¹*Department of Physics, National Central University, Zhongli City, Taoyuan County 32054, Taiwan*

²*Centro de Astrobiología (INTA-CSIC), Carretera de Ajalvir, km 4, Torrejón de Ardoz, 28850 Madrid, Spain*

³*Center for Astrophysics, Harvard & Smithsonian, 60 Garden Street, Cambridge, MA 02138, USA*

⁴*Observatorio Astronmico Nacional (OAN,IGN), Apdo. 112, E-28803 Alcal de Henares, Spain*

(Received November 2, 2018; Revised February 11, 2019; Accepted February 11, 2019)

Submitted to ApJ

ABSTRACT

CO₂ ice has a phase transition at 35 K when its structure changes from amorphous to crystalline. Using Reflection absorption Infrared Spectroscopy (RAIRS), Öberg et al. (2009) observed that the photodesorption yield of CO₂ ice deposited at 60 K and irradiated at 18 K is 40% lower than that of CO₂ ice deposited and irradiated at 18 K. In this work, CO₂ ices were deposited at 16–60 K and UV-irradiated at 16 K to rule out the temperature effect and figure out the relationship between photodesorption yield and ice structure. IR spectroscopy is a common method used for measurement of the photodesorption yield in ices. We found that undetectable C atoms produced in irradiated CO₂ ice can account for 33% of the amount of depleted CO₂ molecules in the ice. A quantitative calibration of QMS was therefore performed to convert the measured ion current into photodesorption yield. During various irradiation periods, the dominant photodesorbing species were CO, O₂, and CO₂, and their photodesorption yields in CO₂ ices deposited at different temperature configurations were almost the same, indicating that ice morphology has no effect on the photodesorption yield of CO₂ ice. In addition, we found that the lower desorption yield reported by Martín-Doménech et al. (2015) is due to a linear relationship between the photodesorption yield and the combination of energy distribution of Microwave-Discharge Hydrogen-flow Lamp (MDHL) and UV absorption cross section of ices.

Keywords: ISM: molecules methods: laboratory: molecular ultraviolet: ISM

1. INTRODUCTION

In the interior of dense clouds, gaseous molecules collide with dust grains and accrete to form ice mantles due to the low dust grain temperature of around 10 K. Desorption of ice molecules induced by cosmic rays and secondary ultraviolet (UV) photons is expected to contribute to the observed gas phase abundances toward cold regions where thermal desorption is inhibited (Muñoz Caro et al. 2016; Öberg et al. 2007b; Westley et al. 1995; Willacy & Millar 1998). The secondary UV field is produced by the interaction of cosmic rays and hydrogen molecules (Cecchi-Pestellini & Aiello 1992; Weinberg et al. 2003; Shen et al. 2004). In general, when

a molecule in the ice bulk absorbs a photon, it becomes excited, and may transfer a fraction of its energy to the molecules near the surface leading to their desorption, which is the so called desorption induced by electronic transition (DIET) (Bertin et al. 2012; Fillion et al. 2014; Martín-Doménech et al. 2015).

CO₂ is one of the most common species in interstellar ices and has been observed toward many high- and low-mass young stellar objects (YSOs), with abundances up to 19%–28% relative to H₂O (Boogert et al. 2015 and references therein). Solid CO₂ is not only a significant chemical tracer of carbon and oxygen in star-forming regions (Van Broekhuizen et al. 2006; van Dishoeck et al. 2006; Cooke et al. 2016), but is an indicator of the temperature history as well (Kim et al. 2012; Pontoppidan et al. 2008).

CO₂ photodesorption has already been the subject of other scientific studies, but its connection with the ice

structure is still not well understood. (Yuan & Yates 2014) discussed the photodesorption rate of CO₂ ice under radiation damage, indicating that the photodesorption yield of CO₂ ice depends on its structure. In addition, the amorphous CO₂ ice provides facile pathways for CO and CO₂ molecules passing through the ice bulk and reaching the surface, which contributes to a more efficient desorption compared to crystalline CO₂ ice (Cooke et al. 2018). (Bahr & Baragiola 2012) measured the photodesorption yields of CO₂ irradiated by Ly α photons at 16–60 K, showing that the photodesorption yield of CO₂ ice strongly depends on temperature. However, CO molecules are efficiently produced in the ice bulk due to CO₂ photodissociation during irradiation. Thermal desorption of photo-produced CO molecules near 30 K may influence the photodesorption of CO₂ above this temperature. In Öberg et al. (2009), the CO₂ deposited at 60 K and cooled down to irradiate at 18 K has a 40% lower photodesorption yield compared to the CO₂ deposited at 18 K, suggesting that the CO₂ photodesorption yield depends on temperature as well as structure. On the other hand, the photodesorption yield of CO ice is found to be linearly temperature dependent between 8–20 K in Muñoz Caro et al. (2016), while the structure of CO ice changed only above 20 K, which means that the photodesorption yield of CO is not directly related to the CO ice structure. In addition to a more efficient photodissociation of CO₂, compared to CO ice, the former is an apolar molecule and the later has a weak dipole moment.

In order to investigate the relationship between the photodesorption yield of CO₂ ice and its morphology, CO₂ ice was deposited at 16 and 30 K to produce amorphous structure whereas deposition at 40, 50, and 60 K served to create crystalline CO₂ ice, since the phase change occurs at \sim 30 K (Escribano et al. 2013). After deposition, the vacuum-ultraviolet (VUV) irradiation of CO₂ ice was done at 16 K to measure the photodesorption yield in the absence of thermal desorption while preserving the initial ice structure. According to Escribano et al. (2013), the morphology of CO₂ ice depends on temperature, which can provide us the temperature history of the environment (d’Hendecourt et al. 1989; Kim et al. 2012; Pontoppidan et al. 2008). In this report, we executed a quantitative calibration of a quadrupole mass spectrometer (QMS) to convert the relative ion current value to a photodesorption yield. Differences in the photodesorption yields between this work and Martín-Doménech et al. (2015) come from the weighted-absorption intensity from the different emission spectra of the VUV lamps, which means the photodesorp-

tion yield is positively proportional to the weighted-absorption intensity.

2. EXPERIMENTAL METHODS

2.1. *Experimental procedure*

The experiments were performed using the Interstellar Photoprocess System (IPS), which includes three parts: the main system, the gas-line and detectors Chen et al. (2014). The main system is an ultra-high-vacuum (UHV) chamber with background pressure $\approx 3 \times 10^{-10}$ torr, equipped with a closed-cycle helium cryostat to cool down the KBr substrate to 16 K. The gas-line is used for preparing CO₂ gas (Matheson Tri-gas, 99.995%) for deposition. The detectors consist of a transmission Fourier transform infrared spectrometer (FTIR) (ABB, FTLA 2000-104) and a quadrupole mass spectrometer (QMS) (MKS Instruments, Microvision 2), which are used to monitor the ice and the desorbing molecules during irradiation, respectively. The column densities of CO₂ ices were controlled to be 140 ± 2 ML (1 ML = 10^{15} molecules cm⁻²). The IR absorption strength adopted for solid CO₂ is 7.6×10^{-17} cm molecule⁻¹ at 2342 cm⁻¹ (Bouilloud et al. 2015; Yamada & Person 1964), and 1.1×10^{-17} cm molecule⁻¹ at 2138 cm⁻¹ for solid CO ice (Jiang et al. 1975).

The energetic VUV photons are generated by the T-type MDHL with an H₂ pressure of 0.4 torr, photon energy from 6.89 to 10.88 eV (180–114 nm), $\approx 4.8 \times 10^{13}$ photon cm⁻² s⁻¹ flux, and 45° incident angle to the substrate. The spectrum of this Microwave-Discharge Hydrogen-flow Lamp (MDHL) has been studied in detail by Chen et al. (2014) and is similar to that of the calculated UV field in dense cloud interiors (Gredel et al. 1989). After cooling down the system to a specific temperature, CO₂ ice was deposited with the pressure at 5×10^{-9} torr for \sim 4 minutes, accompanied by the collection of IR spectra in situ. The VUV irradiation was done at 16 K, and the total irradiation time was 90.5 minutes. During 12 irradiation cycles, the idle intervals were 3 minutes between cycles.

2.2. *Quantitative calibration of mass spectrometer*

CO ice was chosen for quantitative calibration of QMS. The most important characteristic of CO ice is that the conversion efficiency of CO into CO₂ (the only observed photoproduct is CO₂ for a CO ice thickness less than 30 ML) is less than 5% and, in addition, the CO ice photodesorption yield is relatively high (Muñoz Caro et al. 2010). CO ice is, therefore, the best candidate for quantitative calibration of QMS. The experimental procedure of CO ice irradiation is the same as described in Section 2.1, with an ice thickness of 21 ML and VUV

irradiation at 16 K for 1 hour.

In order to correlate the relative signal of QMS ion current measured during photodesorption and the decrease of the CO ice column density, the quantification factor $k_{\text{IPS}}(\text{CO})$ is defined as

$$k_{\text{IPS}}(\text{CO}) = \frac{N(\text{CO})}{A(\text{CO})} \quad (1)$$

where $N(\text{CO})$ is the column density of the photodesorbed CO derived from IR spectra, and $A(\text{CO})$ is the accumulated ion current signal of CO during VUV irradiation. The subscript IPS is used to distinguish the quantification factor $k_{\text{ISAC}}(\text{CO})$ defined by [Martín-Doménech et al. \(2015\)](#), which is reciprocal to the definition of $k_{\text{IPS}}(\text{CO})$ and conducted within InterStellar Astrochemistry Chamber (ISAC). According to [Martín-Doménech et al. \(2015\)](#), the photodesorption of a species can be obtained by comparing to CO and quantified by $k_{\text{IPS}}(\text{CO})$ with the equation:

$$N(\text{mol}) = A(\text{mol}) \times k_{\text{IPS}}(\text{CO}) \times \frac{\sigma^+(\text{CO})}{\sigma^+(\text{mol})} \times \frac{I_F(\text{CO}^+)}{I_F(z)} \times \frac{F_F(28)}{F_F(m)} \times \frac{S(28)}{S(m/z)} \quad (2)$$

where $N(\text{mol})$ is the number of a certain desorbing molecule or atom, $A(\text{mol})$ is the accumulated ion current from QMS, $\sigma^+(\text{mol})$ the ionization cross section for first ionization of the molecule under incident electron energy in QMS, $I_F(z)$ the ionization factor, $F_F(m)$ the fragmentation factor, and $S(m/z)$ is the sensitivity of mass fragment m/z to QMS. The procedure to determine this ratio of sensitivity can be obtained by the ratio of $k_{\text{QMS}} \times S(m/z)$, where k_{QMS} is the proportionality constant, which is independent on species. The procedure of figuring out this ratio is presented in detail in [Martín-Doménech et al. \(2015\)](#), and the corresponding equation is

$$k_{\text{QMS}} \times S(m/z) = 0.14 \times e^{\frac{-m/z}{18.65}} \quad (3)$$

3. RESULTS AND DISCUSSION

3.1. VUV irradiation for CO₂ ice

3.1.1. Photodesorption as seen by the Infrared spectrometer

From IR spectra of CO₂ ices deposited at 16, 30, 40, 50, and 60 K (Figure 1), it is obvious that the structure of CO₂ ice is temperature dependent. From the temperature programmed desorption of pure CO₂ ice, the absorbance of CO₂ changed at ~30 K, which represents the transition to a less amorphous and porous ice ([Escribano et al. 2013](#)). Hence, CO₂ deposited at 16 and 30 K possesses a partially amorphous structure,

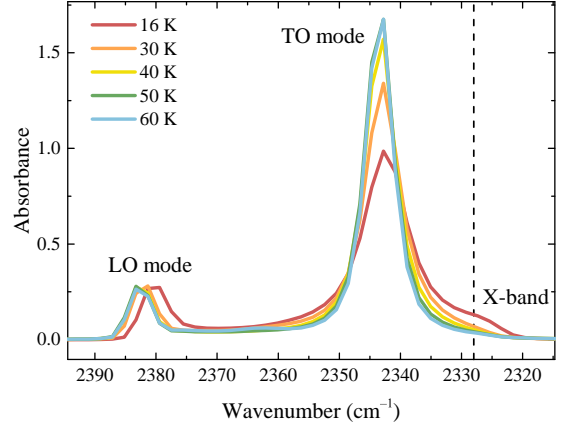


Figure 1. IR absorbances of CO₂ ices at different deposition temperatures. In these experiments, the initial column density of CO₂ was about 140 ML.

whereas it is more ordered and compact at 40, 50, and 60 K configurations. The stretching band (ν_3) of CO₂ is composed of longitudinal optical modes (LO mode, ~2380 cm⁻¹) and transverse optical (TO mode, ~2344 cm⁻¹) since the incident angle of IR beam light is 45 degrees ([Ovchinnikov & Wight 1993](#)). The band at ~2328 cm⁻¹ (usually named X-band) corresponds to a pure and amorphous CO₂ ice structure, which should gradually diminish during irradiation due to the formation of CO and disappear at 30 K during the annealing ([Escribano et al. 2013](#)). The photochemical products can be observed in IR spectra shown in Figure 2. The bands at ~2138 cm⁻¹ and ~2044 cm⁻¹ correspond to CO and CO₃, respectively ([Yamada & Person 1964](#)).

The carbon balance method

$$|\Delta\text{CO}_{2(\text{s})}| = \Delta\text{CO}_{(\text{s})} + \Delta\text{CO}_{3(\text{s})} + \Delta\text{CO}_{(\text{g})} + \Delta\text{CO}_{2(\text{g})} \quad (4)$$

is used to calculate the photodesorption yield of CO₂ ice in IR measurement. The decreasing column density of CO₂ ice should be converted into CO and CO₃ in solid phase, along with the desorbing CO and CO₂ gas phase molecules which can be regarded as photodesorption products. Hence, the total photodesorption yield can be calculated as $|\Delta\text{CO}_{2(\text{s})}| - \Delta\text{CO}_{(\text{s})}$, neglecting the contribution of CO₃ ice since it reached its largest value after 5.5 min of irradiation and became negligible in the later irradiation cycles.

3.1.2. Photodesorption as seen by Mass spectrometer

The photon-induced desorbing species measured by QMS during VUV irradiation are shown in Figure 3. Although QMS is a direct method to measure desorbing species, the measured ion current does not equal to the total number of desorbing molecules because only a

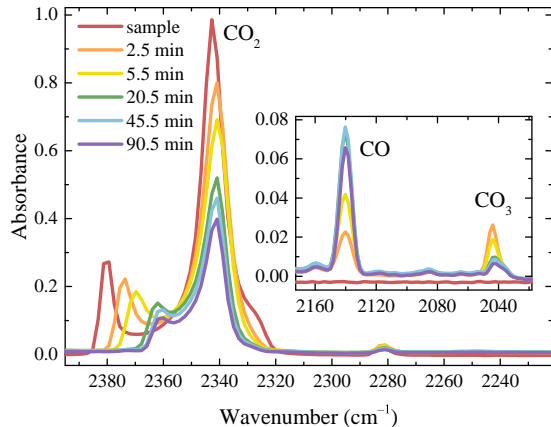


Figure 2. Evolution of the absorbances of CO_2 ($\sim 2340 \text{ cm}^{-1}$), CO ($\sim 2140 \text{ cm}^{-1}$), and CO_3 ($\sim 2044 \text{ cm}^{-1}$) during VUV irradiation at 16 K, with the CO_2 ice deposited at 16 K.

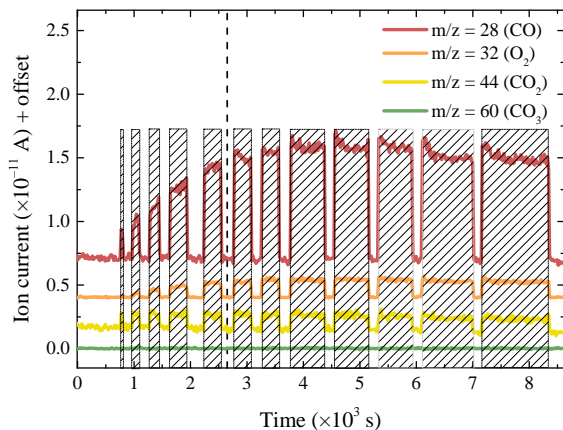


Figure 3. The intensity variation of $m/z = 28$ (CO), 32 (O_2), 44 (CO_2), and 60 (CO_3) during VUV irradiation periods. The dash line represents the photon dose reached $5 \times 10^{16} \text{ photons cm}^{-2}$.

small fraction reaches the QMS. The quantitative values of photodesorption yields from CO_2 deposited at different temperatures can be derived from calibrated QMS described in Section 2.1. After calibration, the integrated signal of each molecule represents the relative photodesorption yield of that given species. The main photo-products are $m/z = 28$ (CO), $m/z = 32$ (O_2), and $m/z = 44$ (CO_2), while no signal for $m/z = 60$ (CO_3) was detected, which is consistent with the result of IR spectra.

Besides the ion current during irradiation, the background signal from ambient environment is also required, which means irradiating the KBr substrate directly before deposition of CO_2 ice. In addition, since gaseous CO_2 is easily dissociated into CO by the ion-

izer of QMS giving $m/z = 28$, we have to extract the mass spectrum of CO_2 measured during deposition. An excess in the relative intensity of $m/z = 28$ during irradiation is, therefore, an indication of CO photon-induced desorption.

3.1.3. The photodesorption mechanisms

There are basically two types of photodesorption mechanisms taking place during the irradiation of a pure CO_2 ice (see also Fillion et al. 2014, Martín-Doménech et al. 2015). One is photochemidesorption, which means that CO_2 is photodissociated to form CO at the surface of CO_2 ice with enough kinetic energy to desorb directly as a CO gas molecule at a decreasing rate with photon dose (concentration of parent molecules is reducing with photon dose). The other one is DIET, which occurs in the ice bulk, as explained in Section 1, and dominates the photodesorption process when both processes take place simultaneously (Bertin et al. 2012; Fillion et al. 2014; Martín-Doménech et al. 2015). The CO or CO_2 molecules inside irradiated CO_2 ice absorb a photon, and transfer its energy sequentially to the molecules near the surface layers to trigger the desorption, which is therefore an indirect photodesorption process.

In the first five irradiation cycles, the ion current signal of $m/z = 28$ is increasing with photon dose (Figure 3), since the number of CO molecules formed during VUV irradiated CO_2 ice are not sufficient to reach the saturation point. This indicates that the CO molecules are photodesorbing through an indirect mechanism, because otherwise the photodesorption yield would be decreasing with photon dose, as explained above. In Figure 4, when photon dose reaches $5 \times 10^{16} \text{ photons cm}^{-2}$, accumulated CO molecules reach 60% of the column density of CO_2 bulk, which is enough to support stably and efficiently the desorption yield via DIET mechanism. On the contrary, CO_2 is the initial ice component and can desorb at constant rate during the whole irradiation sequence even when it is desorbing through the DIET mechanism, because the saturation point is already reached at the beginning of the experiment.

3.2. The discrepancy in the CO_2 photodesorption yield measured by infrared spectrometer and mass spectrometer

In Figure 5, before photon dose reaches $2.5 \times 10^{16} \text{ photons cm}^{-2}$, the IR data shows that the photodesorption rate increases very rapidly (sharp slope), and then decreases gradually, while the QMS data shows the opposite trend. Since the ion current from QMS represents a direct measurement of photodesorbing molecules in the gas phase, the photodesorption yield derived from QMS should be more reliable than the IR results; indeed, the

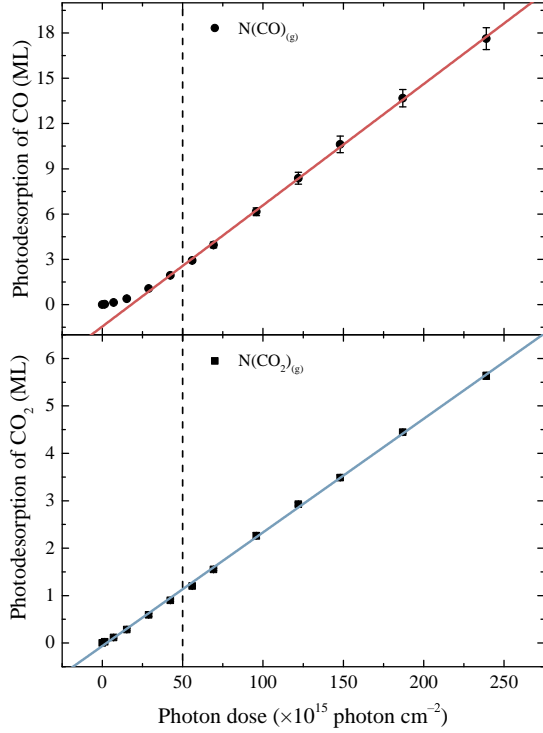
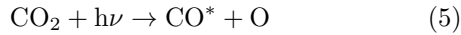


Figure 4. The photodesorption of CO and CO₂ as a function of photon dose in the 16 K deposition and irradiation experiment derived from calibrated QMS.

later measures a decrease in the ice absorption band that can be due to other processes. We propose two possible reasons which may cause this discrepancy: missing carbon and changes in the ice IR absorption strength during irradiation.

3.2.1. Missing Carbon

During VUV irradiation, CO₂ dissociates as



with the dissociation energy 5.45 eV of the C=O double bond (Darwent 1970), which is lower than the energy produced by MDHL (6.89–10.88 eV) to be a feasible reaction. Because the dissociation energy of the so-formed CO molecules (11.09 eV) is larger than the energy provided by the MDHL, one possible back reaction to reform CO₂ is via the predissociation of CO (Gerakines et al. 1996; Loeffler et al. 2005; Muñoz Caro et al. 2010; Okabe et al. 1978): the excited CO* molecule combines with a ground state CO molecule through the reaction

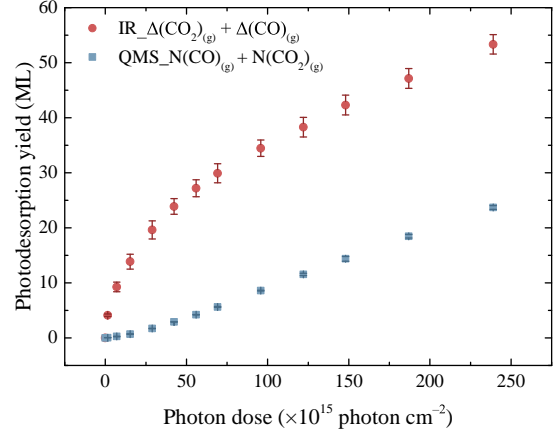
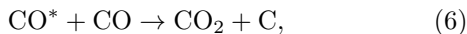


Figure 5. The photodesorption yields derived from IR (carbon balance equation) and QMS as a function of photon dose in 16 K deposition configuration.

producing CO₂ as well as a carbon atom, which is IR-inactive due to the lack of permanent dipole moment. Thus, when the photodesorption yields are calculated by carbon balance method, the carbon atom is not accounted for the calculation of Equation 4, which should be modified as

$$|\Delta\text{CO}_{2(s)}| = \Delta\text{CO}_{(s)} + \Delta\text{CO}_{3(s)} + \Delta\text{C}_{(s)} + \Delta\text{CO}_{(g)} + \Delta\text{CO}_{2(g)} + \Delta\text{C}_{(g)} \quad (7)$$

Accordingly, considering a negligible formation of CO₃ in the thin CO₂ ice irradiation, the total number of CO₂, CO, and C photodesorbing species during the irradiation interval becomes $|\Delta\text{CO}_{2(s)}| - \Delta\text{CO}_{(s)} - \Delta\text{C}_{(s)}$, which is lower than what we derived from carbon balance method, causing a discrepancy of results between IR and QMS. Figure 6 shows evidence that supports the assumption of missing carbon: $A(12) - f_{\text{CO}_2}(12) \times A(\text{CO}_2)$ includes the signal of photodesorption of C atom accompanied with the fragmentation of CO to C, $A(\text{C})/A(\text{CO})$. This ratio is referred to as $f_{\text{CO}}(12)$ for pure CO gas injection into the UHV chamber. $f_{\text{CO}_2}(12)$ is fragmentation of $A(\text{C})/A(\text{CO}_2)$ during CO₂ ice deposition. If the ratio of $[A(12) - f_{\text{CO}_2}(12) \times A(\text{CO}_2)]/A(\text{CO})$ is larger than $f_{\text{CO}}(12)$ during irradiation, it means there exists photodesorption of carbon. In the beginning, photodesorption of carbon atom is high compared to photodesorption of CO, which corresponds to the rapid desorption derived from carbon balance in IR measurement. After the photon dose reaches 1×10^{17} photons cm⁻², the photodesorption of carbon atoms is not so significant, and the amount of solid carbon atoms that remain in the CO₂ ice bulk can be estimated from Equation 7, shown in Figure 7.

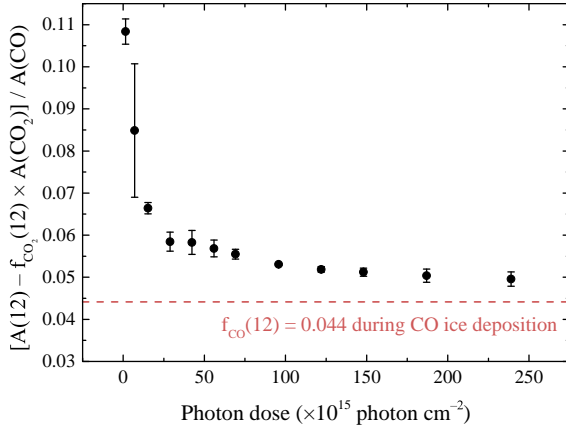


Figure 6. The ratio of $[A(12) - f_{\text{CO}_2}(12) \times A(\text{CO}_2)]/A(\text{CO})$ during VUV irradiation in experiment of CO_2 deposited at 16 K configuration.

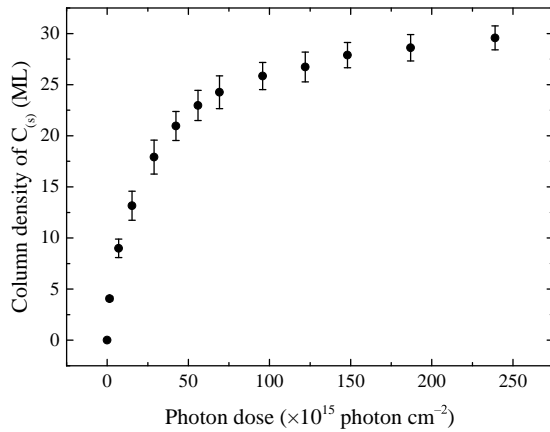


Figure 7. The estimated column density of carbon atom as a function of photon dose in CO_2 deposited at 16 K configuration.

3.2.2. Variation of absorption strength

The high concentration of CO molecules formed during irradiation in the CO_2 ice bulk is expected to cause a change in the CO_2 absorption band strength. Various authors reported changes in the IR band strengths (e.g., d’Hendecourt et al. 1982; Öberg et al. 2007a), as a function of ice composition. We performed the following experiments to confirm whether the absorption strength of CO_2 ice changed during irradiation. CO ice was deposited on substrate first, and then covered by CO_2 ice on top at 16 K, with CO and CO_2 column densities 74 ML and 139 ML ($\text{CO}:\text{CO}_2 = 1:2$), respectively. The layered ice was warmed up from 15 K to 95 K with heating rate of 0.5 K min^{-1} for complete sublimation of CO_2 . During annealing, CO started to thermally diffuse into CO_2 ice through the pores, as described in Cooke

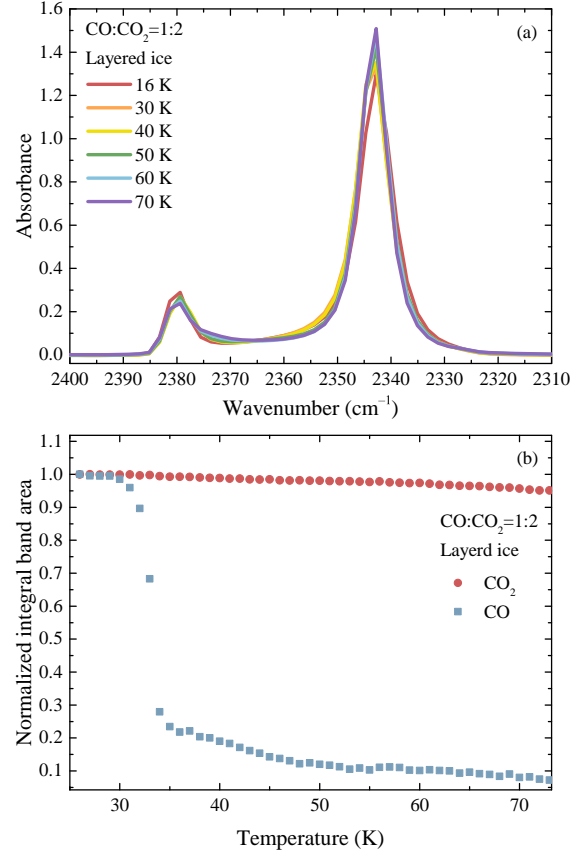


Figure 8. (a) The absorbance of CO_2 during annealing of the $\text{CO}:\text{CO}_2 = 1:2$ layered ice. (b) The normalized integrated IR band of CO and CO_2 during annealing of the $\text{CO}:\text{CO}_2 = 1:2$ layered ice.

et al. (2018). The CO desorbed considerably at 30 K as shown in Figure 8, leaving CO_2 behind.

Furthermore, a mixture of CO and CO_2 ice was deposited to monitor the abundant CO molecules in CO_2 ice, with the similar column density and ratio as in layered ice experiment. During annealing, the CO molecules desorbed gradually from 40–70 K and then $\sim 5\%$ remained in the ice mixture, shown in Figure 9(b). The integrated absorption band of CO_2 changed less than 10% during thermal process, indicating that the variation of absorption strength of CO_2 is not the main cause of discrepancy between the IR and QMS results, even though more than 60% of CO molecules were produced in the CO_2 ice bulk during irradiation.

According to the annealing experiments of CO_2/CO layered ice and CO_2+CO ice mixture, missing carbon is the most likely reason to cause the discrepancy of the trend of photodesorption yields derived from IR spectra and mass spectra. Therefore, we suggest that IR spectroscopy is not suitable for measuring the photodesorp-

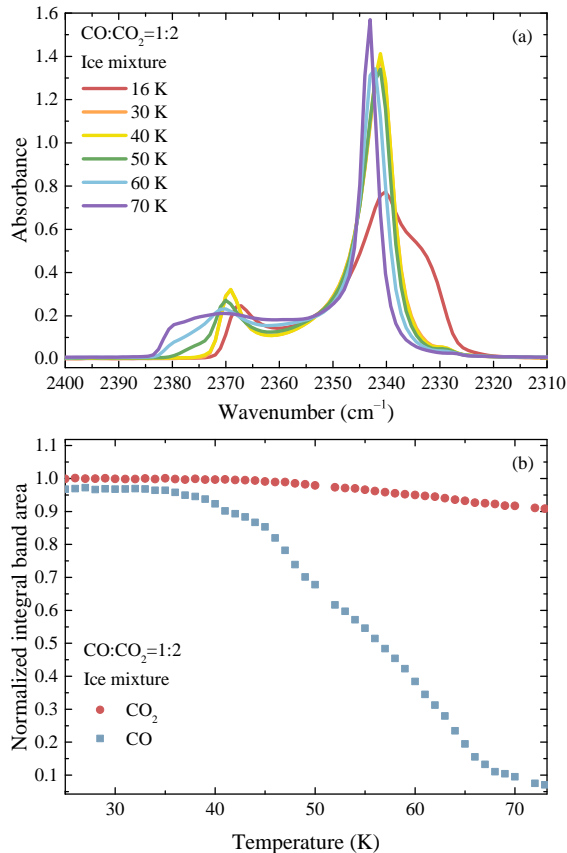


Figure 9. (a) The absorbance of CO_2 during annealing of the $\text{CO}:\text{CO}_2 = 1:2$ ice mixture. (b) The normalized integrated IR band of CO and CO_2 during annealing of the $\text{CO}:\text{CO}_2 = 1:2$ ice mixture.

tion yield of ices which can be easily photodissociated to form molecules or atoms without a dipole moment.

3.3. Photodesorption yield

Owing to the uncertainty of missing carbon in IR measurement and little variation of CO_2 absorption band strength, the photodesorption yields (Y_{pd}) at different deposition temperatures are calculated from the integrated ion current measured from QMS. Through the quantitative calibration of QMS, the photodesorption yield is no longer a relative value, but a meaningful photodesorption yield in units of molecules photon^{-1} . Average values of the photodesorption yield of CO, O_2 , and CO_2 under different deposition temperatures of CO_2 ices are shown in Table 1. From Table 1 it is obvious that CO_2 morphology has no effect on photodesorption yield.

During VUV irradiation, the dominant photodesorbing species are CO and O_2 molecules, in agreement with Bahr & Baragiola (2012) and Martín-Doménech et al.

Table 1. Photodesorption Yields of CO, O_2 , and CO_2 Corresponding to Different Deposition Temperatures of CO_2 Ices

CO_2 deposited temperature (K)	$Y_{\text{pd}}(\text{CO})$ ($\times 10^{-2}$)	$Y_{\text{pd}}(\text{O}_2)$ (molecules photon^{-1})	$Y_{\text{pd}}(\text{CO}_2)$ (molecules photon^{-1})
16	8.3 ± 0.4	2.4 ± 0.1	2.4 ± 0.2
30	7.6 ± 0.4	2.3 ± 0.1	$2. \pm 0.2$
40	8.3 ± 0.4	2.4 ± 0.1	2.4 ± 0.2
50	7.9 ± 0.4	2.3 ± 0.1	2.5 ± 0.2
60	8.3 ± 0.4	2.3 ± 0.1	2.6 ± 0.2
16 ^a	3.4 ± 0.2	1.1 ± 0.1	0.9 ± 0.0
8 ^b	~ 1.20	~ 0.093	$\sim 0.011^c$

NOTE—

^a Experiments with F-type MDHL lamp.

^b Adopted from Martín-Doménech et al. (2015).

^c $^{13}\text{CO}_2$

Table 2. Ratios between Photodesorption Yields of CO/O_2 and CO/CO_2 in the Experiments of $^{12}\text{CO}_2$ and $^{13}\text{CO}_2$ Deposited at 16 and 60 K, Irradiating at 16 K

Deposited temperature Y_{pd} Ratio	16 K		60 K	
	CO/O_2	CO/CO_2	CO/O_2	CO/CO_2
^{12}C	3.39	3.47	3.58	3.13
^{13}C	3.69	3.47	3.88	2.96

(2015). Besides, the value we report for the observed CO_2 photodesorption yield is significantly higher than previous estimates (Bahr & Baragiola 2012; Fillion et al. 2014; Martín-Doménech et al. 2015). We, therefore, employed $^{13}\text{CO}_2$ ice, deposited at 16 and 60 K, to discard a potential contamination of CO_2 in the chamber, followed by irradiation at 16 K following the experimental procedure of $^{12}\text{CO}_2$ described in Section 2.1. The ratios between photodesorption yields of CO/O_2 and CO/CO_2 at 16 and 60 K shown in Table 2 are almost the same in both $^{12}\text{CO}_2$ and $^{13}\text{CO}_2$ cases, which corroborates that the photodesorption yield of CO_2 is comparable to that of O_2 in our experiments.

Photodesorption yield is dependent on the VUV-absorption cross section of the species and the VUV spectrum of MDHL. From Table 1, there is a large discrepancy of photodesorption yields of CO, O_2 , and CO_2 between Martín-Doménech et al. (2015) and this work. Chen et al. (2014) reported that the geometry of quartz-tube of MDHL leads to different VUV spectra. We adopted a T-type lamp in IPS whereas a F-type lamp was used in ISAC (Martín-Doménech et al. 2015). In addition, experiments using a F-type lamp were also performed in IPS. The pho-

photodesorption yields are shown in Table 1. According to Beer-Lambert law, the absorption spectrum of CO₂ ice is

$$I_{abs}(\text{CO}_2) = I_0 - I_t = I_0(1 - e^{-N\sigma_{\text{CO}_2}}), \quad (8)$$

where I_0 and I_t is the intensity of incidence and transmittance as a function of wavelength λ , N is the column density of CO₂ ice, and σ_{CO_2} the VUV-absorption cross section of CO₂ as a function of wavelength λ .

The normalized incident intensity in three kinds of MDHL configurations are shown in Figure 10(a), while (b) depicts the VUV-absorption cross section of CO, O₂, and CO₂. The weighted-absorption intensity of CO₂ in three kinds of MDHL configurations derived from Equation 8 are shown in Figure 10(c). The integration of CO₂ absorption spectrum is positively correlated to the photodesorption, which is a zeroth-order process since it is not dependent on thickness in the thin ice experiments (Cottin et al. 2003). Figure 11(a) displays the photodesorption yields of CO₂ as a function of integrated VUV absorption of CO₂ convolved with the emission from the three kinds of MDHL configurations, which is represented by a linear relationship.

CO is a photo-dissociation product from CO₂ ice, and photon-induced desorption took place mainly through the DIET mechanism (Martín-Doménech et al. 2015), therefore the photodesorption yield of CO is proportional to the product of integrated absorption spectrum of CO₂ (production yield of CO molecules in CO₂ ice) and integrated absorption spectrum of CO (energy transfer from excited CO molecules to those CO molecules in top few monolayers), shown in Figure 11(b). As for O₂, the formation is also a two-step reaction including Equation 5 and



Analogous to the case of CO, the photodesorption of O₂ is proportional to the multiplication of integrated absorption spectra of CO₂ and that of O₂, shown in Figure 11 (c).

4. CONCLUSIONS AND ASTROPHYSICAL IMPLICATIONS

We have investigated the photodesorption yield of CO₂ as a function of ice deposition temperature by transmittance FTIR and mass spectrometry. From IR spectral analysis, it is possible to estimate the total photodesorption yield of all the desorbing species, but information on the desorption of individual species cannot be extracted from this data alone. Moreover, we have demonstrated that the IR absorption strength of

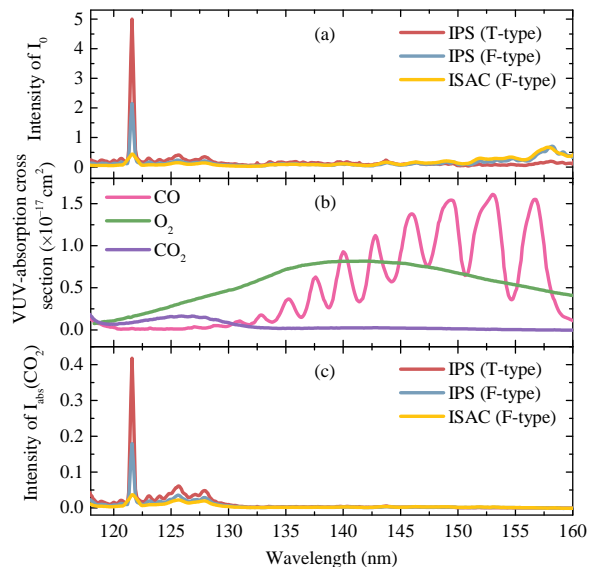


Figure 10. (a) The incident intensity I_0 in three kinds of MDHL configurations. (b) VUV-absorption cross section of CO, O₂, and CO₂. (c) The weighted-absorption intensity of CO₂ in three kinds of MDHL configurations.

CO₂ does not change significantly during irradiation. Therefore, the apparent discrepancy in the estimated photodesorption yields, obtained by IR and QMS, is explained when the IR-inactive carbon atoms formed by CO₂ photoprocessing are taken into account. These carbon atoms reside in the CO₂ ice bulk. With regard to the uncertainty in the photodesorption yield, we have performed a novel method for quantitative calibration of the mass spectrometer to study the photodesorption yield of CO₂ ice deposited at different temperatures. The quantitative calibration of QMS is significant and indispensable to investigate the photodesorption yields. CO, O₂, and CO₂ are the dominant desorbing species with the following photodesorption yields: $Y_{pd}(\text{CO}) = 8.3 \pm 0.4 \times 10^{-2}$ molecules photon⁻¹, $Y_{pd}(\text{O}_2) = 2.3 \pm 0.1 \times 10^{-2}$ molecules photon⁻¹, and $Y_{pd}(\text{CO}_2) = 2.4 \pm 0.2 \times 10^{-2}$ molecules photon⁻¹. The apparent discrepancy in the photodesorption yields between this work and Martín-Doménech et al. (2015) can be explained very well by the linear relationship between the photodesorption yield and the integrated VUV-absorption in three kinds of MDHL configurations. In Öberg et al. (2009), the $Y_{pd}(\text{CO}_2)$ for CO₂ deposited at 18-30 K is 2.3×10^{-3} molecules photon⁻¹ calculated from $1.2 \times 10^{-3} \times (1 - e^{-x/2.9}) + 1.1 \times 10^{-3} \times (1 - e^{-x/4.6})$, where x is the ice thickness, i.e., $x = 141$ ML to compare with this work. The $Y_{pd}(\text{CO}_2)$ is 40% lower for

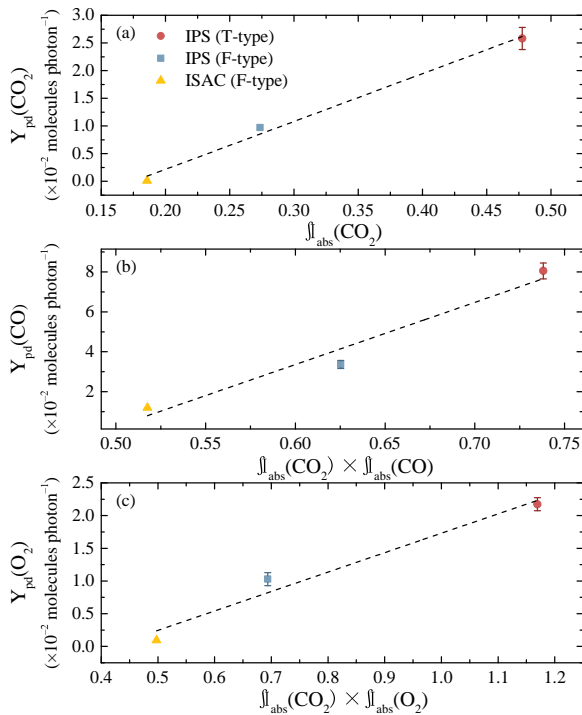


Figure 11. The photodesorption yields of (a) CO_2 , (b) CO , and (c) O_2 as a function of (a) $\int I_{abs}(\text{CO}_2)$, (b) $\int I_{abs}(\text{CO}_2) \times I_{abs}(\text{CO})$, (c) $\int I_{abs}(\text{CO}_2) \times I_{abs}(\text{O}_2)$ in three kinds of MDHL configurations with a linear fit.

CO_2 deposited at 60 K and cooled down to 18 K than that for CO_2 deposited at 18 K. This seems to verify that in the case of CO_2 deposited at 40–60 K, the UV photon energy contributed to restructure the ice from crystalline to amorphous to make an effective exit channel for molecules to desorb to the surface, in line with the conclusion from Yuan & Yates (2014). In contrast, this study demonstrates that the photodesorption yield of CO_2 is not ice structure dependent, which is incompatible with the preceding works based on IR spectroscopy for quantification (Öberg et al. 2009; Yuan & Yates 2014). As mentioned in Muñoz Caro et al. (2016), the photodesorption yield of CO ice is independent of ice structure, and the linearly decreasing photodesorption yield for increasing deposition temperature might be due to orientational disorder. Therefore, whether polar CO or non-polar CO_2 , their structures are not directly related to the photodesorption yield.

This work has implications for the interpretation of gas-phase observations toward cold interstellar and circumstellar environments where ice mantles were submitted

to UV irradiation. The ice analog component studied in this paper, pure CO_2 ice, is believed to form in ice mantles by two processes. One is the CO_2 segregation out of the CO_2 - H_2O mixture, leading to CO_2 inclusions in water ice. The other is a distillation process, in which CO evaporates from a CO_2 - CO ice mixture, leaving pure CO_2 behind (Kim et al. 2012; Pontoppidan et al. 2008). In the former process, UV irradiation of CO_2 inclusions in water ice produces CO , O_2 and CO_3 molecules that will be mainly retained in the ice with a negligible desorption. The latter evolutionary phase of the ice is favorable for the photodesorption of CO_2 , because CO_2 ice is exposed to the surface of ice mantles, and our experimental results are more directly applicable to this scenario. Only CO_3 is not expected to photodesorb in this case, according to the experiments. In particular, the photodesorption yields of CO_2 , the CO and O_2 photoproducts, in molecules photon $^{-1}$, should be valid to estimate the density of these species in the gas of cold environments. In dense clouds, the secondary UV field originated by excitation of molecular hydrogen is about $10^3 - 10^4$ photons $\text{cm}^{-2} \text{s}^{-1}$, and should be dominated by the molecular emission lines with a smaller contribution of the more energetic Ly- α photons produced by atomic hydrogen. This UV emission spectrum, along with the total value of the UV flux, dictates the values of the photodesorption yields in our experiments. In Section 3.3 of this paper, we report the linear dependence of the photodesorption yields with the UV lamp emission and ice absorption spectra in the UV.

Pure CO_2 ice is expected to be in the crystalline form in ice mantles, since the band around $4.30 \mu\text{m}$ (2328 cm^{-1}) of amorphous CO_2 ice is absent in the observed spectra toward dense clouds and protostars; this suggests that CO_2 ice was formed on the dust at temperatures above 25 K, or was submitted later on to these temperatures (Escribano et al. 2013). We confirmed that this ice structure reflects the temperature of ice deposition in the experiments. One of the conclusions from our work is that the photodesorption yield of CO_2 does not depend on the degree of amorphous or crystalline structure of the ice.

In Section 3.2 of this paper, missing carbon is introduced to explain the CO_2 discrepancy in the photodesorption yield measured by infrared spectrometer and mass spectrometer. When carbon atom is considered in the carbon balance method, the estimated ratio of $\Delta C_{(s)}/\Delta \text{CO}_{2(s)}$ is $\sim 33\%$. Unlike CO_2 , other C-bearing molecules present in ice mantles, in particular CO , CH_3OH , and CH_4 , are not expected to contribute appreciably to the release of C atoms in the gas phase. In the case of CO , only the most energetic photons with

$E > 11$ eV are capable to dissociate CO molecules to produce C. Meanwhile, photoprocessing of simple hydrocarbons in the ice, like CH₃OH or CH₄, trigger the formation of numerous species and no free C atoms are produced.

A possible C-chemistry driven by secondary-UV in CO₂-rich ice will be a minor effect compared to X-rays, in particular in thin ices. But a considerable amount of C retained in the ice bulk, and close to the surface as in one of the ice scenarios (the one where CO distillates near 20 K and CO₂ is the main component on the ice mantle surface), could have implications for the evolution of dense cloud interiors, and later on during star-formation. Indeed, the [C I] line was found to be a more important coolant than the lowest three rotational transitions of CO in moderate density gas, $n(\text{H}_2) \sim$ a few 10^3 cm^{-3} as long as $N(\text{C})/N(\text{CO}) \sim 0.1$ (Pineau des Forêts et al. 1992; Wilson 1997). However, the ratios C/CO and C+/CO drop sharply when n_{H} approaches 10^4 cm^{-3} (Pineau des Forêts et al. 1992). Therefore, the background radiation field ionizes neutral C atoms, and C II is regarded to be an efficient coolant of the gas in star-forming regions within dense clouds (e.g. Stahler & Palla 2008).

The release of C atoms to the gas phase might also have important implications for chemistry. At very low gas temperatures, neutral-neutral reactions are slow and C can stay longer in its atomic form, while at high temperatures, C will react with neutrals forming CO, HCN, C₂, etc.; see, for instance, the KIDA database

(<http://kida.obs.u-bordeaux1.fr/>).

Carbon-chain molecules account for $\sim 40\%$ of the interstellar molecular species detected to date, being specially abundant in dark clouds. The starless core Taurus Molecular Cloud-1 Cyanopolyyne Peak (TMC-1 CP) is the richest known source of carbon-chain molecules and is where most of the carbon-chain molecules detected in interstellar clouds exist (e.g., Foss et al. 2001, Kaifu et al. 2004). Recently, carbon-chain molecules have also been detected in dense and warm regions around low-mass protostars. The carbon-chain molecules are thought to be produced from CH₄ evaporated from dust grains via a mechanism called warm carbon-chain chemistry (WCCC), for which representative sources are L1527 and IRAS 15398-3359 (e.g., Sakai et al. 2008). The enhancement of carbon-chain molecules in these regions has been interpreted as the consequence of the evaporation of CH₄ in a lukewarm (TK ~ 50) region near a protostar (Hassel et al. 2008; Aikawa et al. 2008). The release of atomic C in this warm region might be an important ingredient for the chemical evolution of these objects.

This work has been supported by the MOST grants MOST 107-2112-M-008-016-MY3 (Y-JC), Taiwan, and project from the Spanish Ministry of Science, Innovation and Universities supported this research under grant number AYA2017-85322-R (AEI/FEDER, UE), and MDM-2017-0737 Unidad de Excelencia Mara de Maeztu– Centro de Astrobiología (INTA-CSIC).

REFERENCES

- Aikawa, Y., Wakelam, V., Garrod, R. T., & Herbst, E. 2008, *ApJ*, 674, 984
- Bahr, D., & Baragiola, R. 2012, *ApJ*, 761, 36
- Bertin, M., Fayolle, E. C., Romanzin, C., et al. 2012, *PCCP*, 14, 9929
- Boogert, A. A., Gerakines, P. A., & Whittet, D. C. 2015, *ARA&A*, 53, 541
- Bouilloud, M., Fray, N., Bénilan, Y., et al. 2015, *MNRAS*, 451, 2145
- Cecchi-Pestellini, C., & Aiello, S. 1992, *MNRAS*, 258, 125
- Chen, Y.-J., Chuang, K.-J., Muñoz Caro, G. M., et al. 2014, *ApJ*, 781, 15
- Cooke, I. R., Fayolle, E. C., & Öberg, K. I. 2016, *ApJ*, 832, 5
- Cooke, I. R., Öberg, K. I., Fayolle, E. C., Peeler, Z., & Bergner, J. B. 2018, *ApJ*, 852, 75
- Cottin, H., Moore, M. H., & Bénilan, Y. 2003, *ApJ*, 590, 874
- Darwent, B. d. 1970, Bond dissociation energies in simple molecules, Tech. rep., National Standard Reference Data System
- d’Hendecourt, L., Allamandola, L., Baas, F., & Greenberg, J. 1982, *A&A*, 109, L12
- d’Hendecourt, L., Jourdain de Muizon, M., et al. 1989, *A&A*, 223, L5
- Escribano, R. M., Caro, G. M. M., Cruz-Díaz, G. A., Rodríguez-Lazcano, Y., & Maté, B. 2013, *PNAS*, 110, 12899
- Fillion, J.-H., Fayolle, E. C., Michaut, X., et al. 2014, *FaDi*, 168, 533
- Gerakines, P., Schutte, W., & Ehrenfreund, P. 1996, *A&A*, 312, 289
- Gredel, R., Lepp, S., Dalgarno, A., & Herbst, E. 1989, *ApJ*, 347, 289
- Hassel, G. E., Herbst, E., & Garrod, R. T. 2008, *ApJ*, 681, 1385

- Jiang, G. J., Person, W. B., & Brown, K. G. 1975, *JChPh*, 62, 1201
- Kim, H. J., Evans II, N. J., Dunham, M. M., Lee, J.-E., & Pontoppidan, K. M. 2012, *ApJ*, 758, 38
- Loeffler, M., Baratta, G., Palumbo, M., Strazzulla, G., & Baragiola, R. 2005, *A&A*, 435, 587
- Martín-Doménech, R., Manzano-Santamaría, J., Muñoz Caro, G. M., et al. 2015, *A&A*, 584, A14
- Muñoz Caro, G. M., Chen, Y.-J., Aparicio, S., et al. 2016, *A&A*, 589, A19
- Muñoz Caro, G. M., Jiménez-Escobar, A., Martín-Gago, J., et al. 2010, *A&A*, 522, A108
- Öberg, K. I., Fraser, H. J., Boogert, A. A., et al. 2007a, *A&A*, 462, 1187
- Öberg, K. I., Fuchs, G. W., Awad, Z., et al. 2007b, *ApJL*, 662, L23
- Öberg, K. I., Van Dishoeck, E. F., & Linnartz, H. 2009, *A&A*, 496, 281
- Okabe, H., et al. 1978, *Photochemistry of small molecules*, Vol. 431 (Wiley New York)
- Ovchinnikov, M. A., & Wight, C. A. 1993, *JChPh*, 99, 3374
- Pineau des Forêts, G., Roueff, E., & Flower, D. 1992, *MNRAS*, 258, 45P
- Pontoppidan, K. M., Boogert, A. C., Fraser, H. J., et al. 2008, *ApJ*, 678, 1005
- Sakai, N., Sakai, T., Hirota, T., & Yamamoto, S. 2008, *ApJ*, 672, 371
- Shen, C., Greenberg, J., Schutte, W., & Van Dishoeck, E. 2004, *A&A*, 415, 203
- Stahler, S. W., & Palla, F. 2008, *The formation of stars* (John Wiley & Sons)
- Van Broekhuizen, F., Groot, I., Fraser, H., van Dishoeck, E., & Schlemmer, S. 2006, *A&A*, 451, 723
- van Dishoeck, E. F., Jonkheid, B., & van Hemert, M. C. 2006, *Faraday Discussions*, 133, 231
- Weinberg, D., Davé, R., Katz, N., & Kollmeier, J. 2003, in *AIP Conf. Ser.*, Vol. 666, 157
- Westley, M., Baragiola, R., Johnson, R., & Baratta, G. 1995, *P&SS*, 43, 1311
- Willacy, K., & Millar, T. 1998, *MNRAS*, 298, 562
- Wilson, C. D. 1997, *ApJL*, 487, L49
- Yamada, H., & Person, W. B. 1964, *JChPh*, 41, 2478
- Yuan, C., & Yates, J. T. J. 2014, *ApJ*, 780, 8